LETTERS
PUBLISHED ONLINE: 9 MARCH 2014 | DOI: 10.1038/NNANO.2014.27
nature nanotechnology

Third-harmonic-upconversion enhancement from a single semiconductor nanoparticle coupled to a plasmonic antenna

Heykel Aouani[1†*], Mohsen Rahmani[1†], Miguel Navarro-Cía[2] and Stefan A. Maier[1]

The ability to convert low-energy quanta into a quantum of higher energy is of great interest for a variety of applications, including bioimaging[1], drug delivery[2] and photovoltaics[3]. Although high conversion efficiencies can be achieved using macroscopic nonlinear crystals, upconverting light at the nanometre scale remains challenging because the subwavelength scale of materials prevents the exploitation of phase-matching processes[4]. Light–plasmon interactions that occur in nanostructured noble metals have offered alternative opportunities for nonlinear upconversion of infrared light, but conversion efficiency rates remain extremely low due to the weak penetration of the exciting fields into the metal[5]. Here, we show that third-harmonic generation from an individual semiconductor indium tin oxide nanoparticle is significantly enhanced when coupled within a plasmonic gold dimer. The plasmonic dimer acts as a receiving optical antenna[6], confining the incident far-field radiation into a near field localized at its gap; the indium tin oxide nanoparticle located at the plasmonic dimer gap acts as a localized nonlinear transmitter upconverting three incident photons at frequency ω into a photon at frequency 3ω. This hybrid nanodevice provides third-harmonic-generation enhancements of up to 10^6-fold compared with an isolated indium tin oxide nanoparticle, with an effective third-order susceptibility up to 3.5×10^3 nm^2 V^{-2} and conversion efficiency of 0.0007%. We also show that the upconverted third-harmonic emission can be exploited to probe the near-field intensity at the plasmonic dimer gap.

Coherent conversion processes occurring at the macroscale are intensively exploited for upconverting tunable laser light[7] and for fast label-free imaging of biological samples[8]. At nanoscopic scales, luminescence upconversion subwavelength crystals can play the role of carriers for intracellular drug delivery[9] and are considered to be promising candidates for overcoming the Shockley–Queisser efficiency limit of single-junction solar cells[3,10]. Upconversion of infrared pulsed light within nanometric volumes can also be achieved through the exploitation of coherent harmonic generation processes from plasmonic structures excited at resonance[5]. Although most seminal works have focused on the nonlinear intrinsic responses from plasmonic structures[11–13], only a few recent studies have investigated the enhanced nonlinear extrinsic responses provided by plasmonic couplings[4]. Such configurations are particularly suitable for electrical[14] and optical[15] control of nonlinear properties from bulk materials adjacent to plasmonic structures, or for plasmon-enhanced generation of coherent extreme-ultraviolet light from gas jets[16]. However, despite significant advances, achieving high harmonic conversion efficiencies of light from nonlinear nanostructured materials remains a challenge.

We experimentally demonstrate the viability of a novel subwavelength harmonic conversion system made of a single indium tin oxide (ITO) nanoparticle decorated with a plasmonic dimer (Fig. 1a). Although the third harmonic generation (THG) from an isolated ITO nanoparticle is relatively weak, localized plasmonic coupling dramatically enhances, by several orders of magnitude, its three-photon upconversion, which enables the unambiguous discrimination of the third harmonic signal from the ITO nanoparticle from the strong intrinsic nonlinear metallic background[17–19]. Due to the non-absorbing nature of the nonlinear generation processes, the third harmonic scattering from the ITO nanoparticle is mainly sensitive to the local intensity excitation in the plasmonic gap region, thus enabling an accurate probing of near-field intensities with a far-field method.

The nonlinear upconversion nanosystems were realized by means of two-step electron-beam lithography and a combination of etch-down and lift-off methods, with well-controlled spatial alignment. Single 25-nm-diameter ITO nanoparticles were generated by ion-beam etching followed by a lift-off procedure to create well-aligned gold dimer decorations (Fig. 1b). This led to the completion of the nonlinear upconversion system comprising an ITO nanoparticle at the gap of a plasmonic dimer, as presented in Fig. 1b,c. Owing to the non-directional deposition nature of the ITO sputtering process, the combination of etch-down and lift-off methods is essential to realize the hybrid nanostructures presented in this work, hence the differences in the fabrication approach compared with those used recently for subwavelength plasmonic mapping[20,21] and probing[22] investigations, or for controlling the optical responses of plasmonic antennas by nanomaterial loading[23].

Finite-difference time-domain (FDTD) simulations exploiting the total-field scattered-field (TFSF) formulation are performed to provide the spatial distribution of the intensity enhancement and extinction spectrum of the fabricated dimers (Fig. 1d,e). The dimer models are generated from scanning electron microscopy (SEM) images such as the one presented in Fig. 1c, and the ITO nanoparticles are considered ideal 25-nm-diameter cylinders localized at the position determined from the SEM pictures. The optical dielectric functions of Au, Cr (adhesion layer), SiO_2 (substrate) and ITO are fitted to experimental data[24,25]. As highlighted in previous works[26], the introduction of a dielectric nanoparticle at the gap of a metallic optical antenna dimer leads to a spectral redshift of its plasmonic resonance (Fig. 1e).

The linear experimental characterization of the fabricated structures in an array configuration (112 nanostructures per array, pitch

[1]The Blackett Laboratory, Department of Physics, Imperial College London, London SW7 2AZ, UK, [2]Optical and Semiconductor Devices Group, Department of Electrical and Electronic Engineering, Imperial College London, London SW7 2BT, UK; [†]These authors contributed equally to this work.
*e-mail: h.aouani@imperial.ac.uk

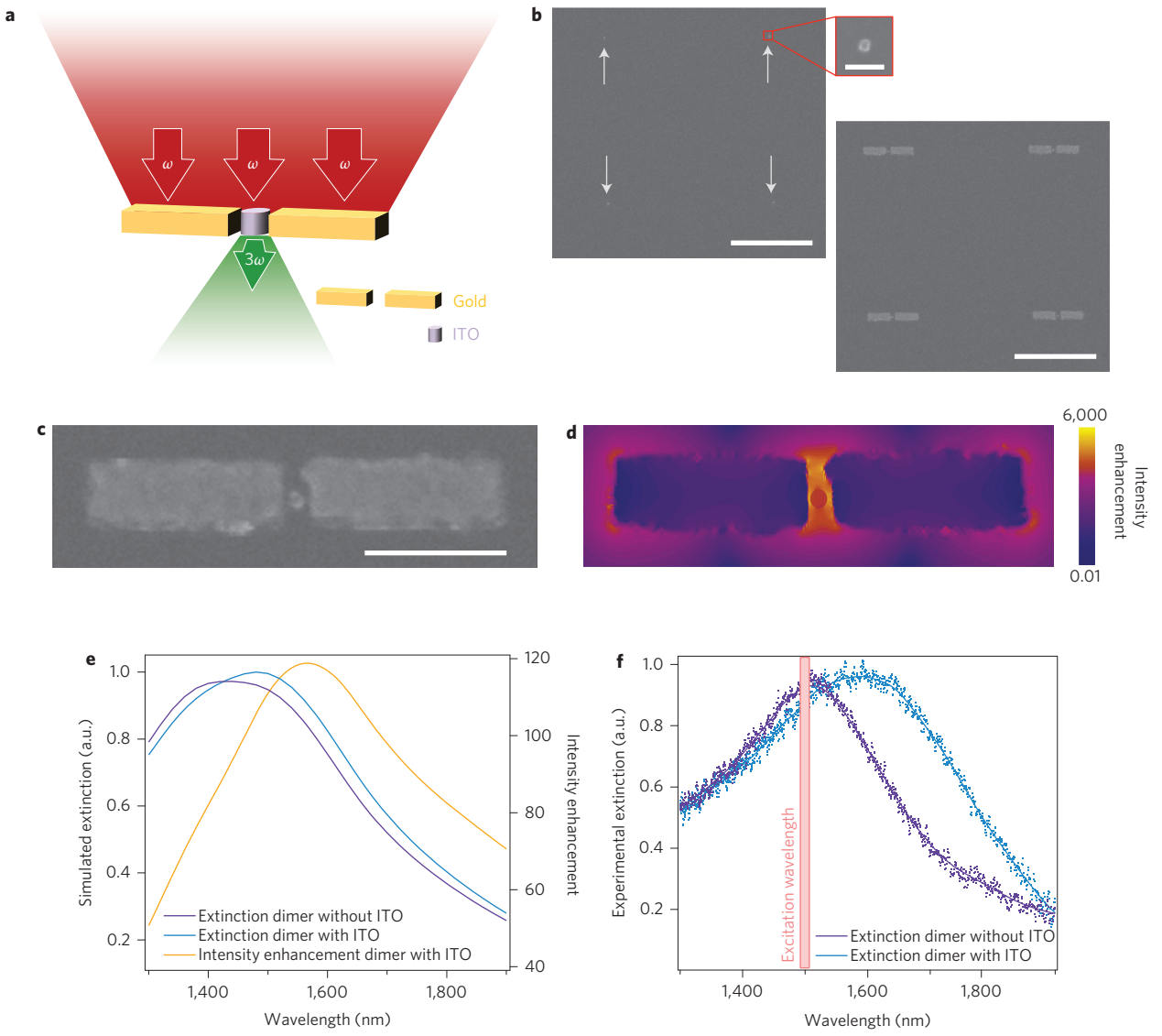

Figure 1 | Nonlinear upconversion nanosystem. a, Schematic of third-harmonic radiation from a single ITO nanoparticle decorated with a plasmonic nanorod dimer. For clarity, we show a transmission configuration, but in our experiment we collected the backward-emitted third-harmonic signal. **b**, SEM images of an array of upconversion systems. In a first step, 25 nm dots are generated using an etch-down method (left). In a second step, the gold dimer decoration is created using a lift-off procedure (right). Arrows in the left SEM image indicate the positions of the ITO nanoparticles. Scale bars: main images, 1 μm; inset, 100 nm. **c**, SEM image of a single nonlinear upconversion system. Scale bar, 200 nm. **d**, FDTD computation of intensity enhancement along the middle cross-sectional plane for $\lambda = 1{,}500$ nm and an incident plane-wave polarized parallel to the dimer axis. **e**, Simulated extinction cross-section of the 35-nm-gap nanorod dimer with and without an ITO nanoparticle at its gap, and intensity enhancement at the centre of the ITO nanoparticle when coupled to the plasmonic dimer. **f**, Experimental extinction cross-section of the 35-nm-gap nanorod dimer array with and without an ITO nanoparticle at its gap. The red shaded area indicates the spectral position of the fundamental excitation wavelength used for the nonlinear measurements.

of 2 μm) was performed using a commercial Fourier-transform infrared spectroscopy (FTIR) apparatus (see Supplementary Section 2 for details). The corresponding extinction spectra (defined as 1-transmission) for the 35 nm gap nanorod dimer with and without an ITO nanoparticle at its gap is presented in Fig. 1f. A slight redshift of the resonance peak position is observed for both configurations when compared with the numerical predictions of Fig. 1e. This can be attributed to minor defects related to the fabrication process (thickness of the gold layer, roughness and so on), but the shapes of the measured extinction cross-sections agree well with the simulated spectra. From Fig. 1f, one can also observe that the fundamental excitation wavelength set for the nonlinear investigations matches the plasmonic resonance of the nanorod dimer not coupled to an ITO nanoparticle.

We started our nonlinear experimental investigations by measuring the THG from an isolated ITO nanoparticle (see Supplementary Section 3 for details). Under excitation at frequency ω, the third-order ITO susceptibility[25] $\chi^{3\omega} = 3.36\ \mathrm{nm^2\ V^{-2}}$ induces a nonlinear polarization $\mathbf{P}^{3\omega} = \varepsilon_0 \chi^{3\omega} \mathbf{E}^{\omega} \mathbf{E}^{\omega} \mathbf{E}^{\omega}$ (ε_0 is the permittivity of free space and $\mathbf{E}^{\omega}$ is the incident electric field at frequency ω), which in turns generates a radiation of intensity $I^{3\omega} \propto |\mathbf{P}^{3\omega}|^2$. As expected, a fundamental femtosecond excitation at $\lambda = 1{,}500$ nm gives rise to the instantaneous third-harmonic ITO response centred at $\lambda = 500$ nm presented in Fig. 2a. From this spectrum, the THG radiated power is estimated to be 1.94×10^{-20} W, corresponding to an upconversion efficiency of 5.8×10^{-10}%. This weak efficiency is dramatically enhanced when the single ITO nanoparticle is decorated with a 35-nm-gap nanorod plasmonic dimer (Fig. 2b) under parallel polarized excitation. The third-harmonic peak intensity

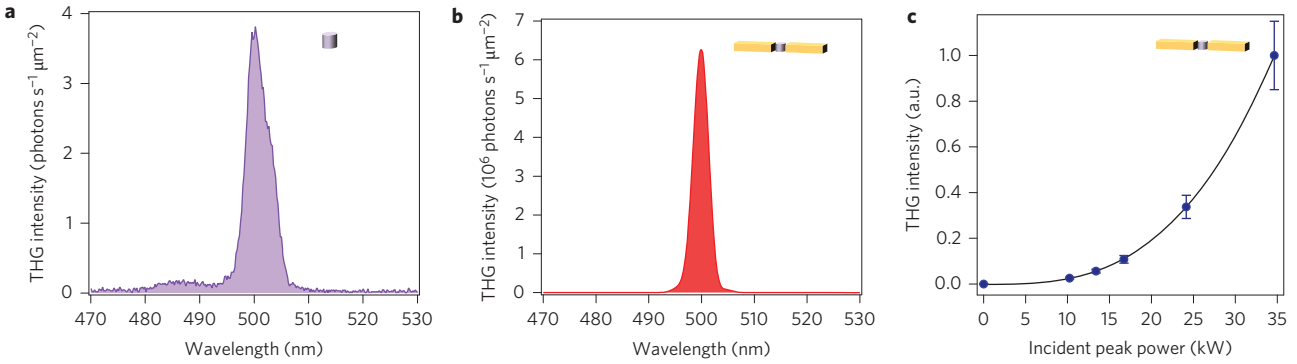

Figure 2 | Three-photon upconversion enhancement from a single ITO nanoparticle decorated with a plasmonic dimer. a, Third-harmonic generation spectrum of an isolated 25 nm ITO nanoparticle for an incident wavelength at 1,500 nm (average incident power of 50 µW, peak intensities of 45.7 GW cm^{-2}). **b**, Third-harmonic generation spectrum of a single ITO nanoparticle localized at the centre of a 35-nm-gap nanorod dimer under parallel polarized excitation (average incident power of 50 µW, peak intensities of 45.7 GW cm^{-2}). **c**, Evolution of third-harmonic intensity as a function of fundamental incident power. Blue symbols indicate experimental data. Black line is a numerical fit with a third-order power function. The error bars displayed indicate the standard deviation of the measurements.

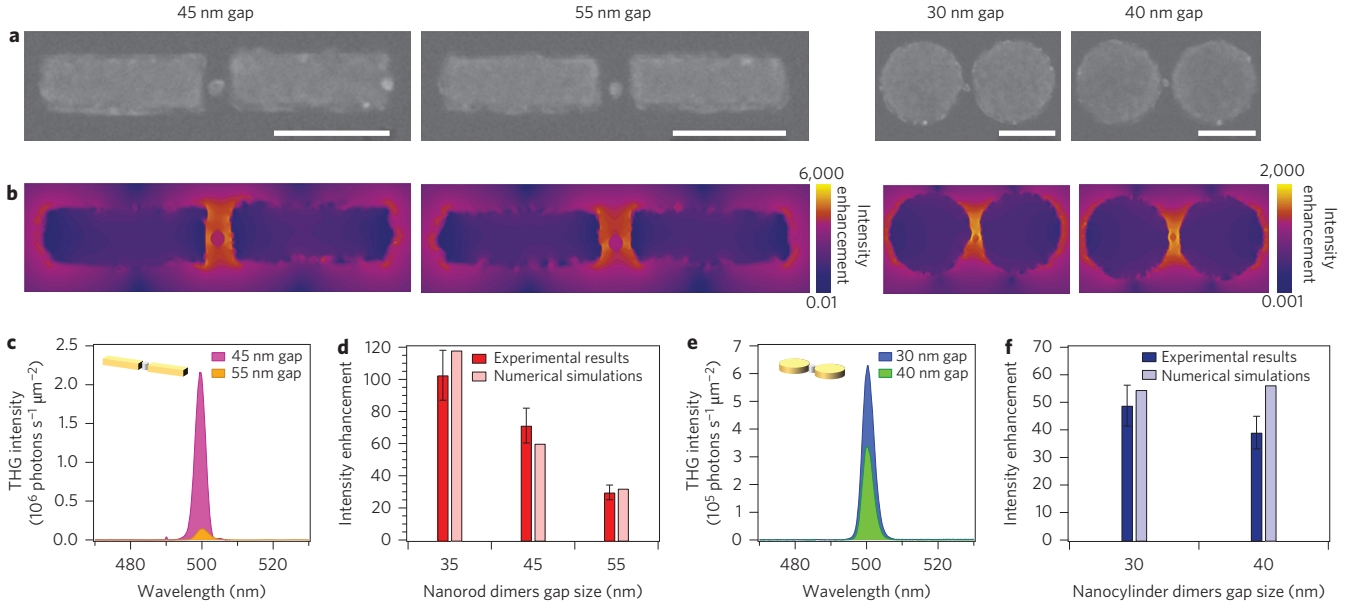

Figure 3 | Probing plasmonic hot spots with a nanoscale nonlinear particle. a, SEM images of a single nonlinear upconversion system for various plasmonic dimer geometries. Scale bars, 200 nm. **b**, FDTD intensity enhancement maps at the middle cross-sectional plane corresponding to the SEM images in **a**. **c**, Third-harmonic spectrum of an ITO nanoparticle localized in 45-nm- and 55-nm-gap nanorods. **d**, Electric field intensity enhancement at the gap of nanorod dimers for gaps of various sizes. **e**, Third-harmonic spectrum of an ITO nanoparticle localized in 30-nm- and 40-nm-gap nanocylinders. **f**, Electric field intensity enhancement at the gap of nanocylinder dimers with different gap size.

generated by the hybrid upconversion system is increased by six orders of magnitude compared with an isolated ITO nanoparticle, leading to a third-harmonic power of 2.17×10^{-14} W and an upconversion efficiency of 7×10^{-4}%. Note that, unlike the linear characterization performed by FTIR spectroscopy, all nonlinear measurements with hybrid nanostructures have been conducted on single entities. Such a huge increase in the nonlinear signal essentially results from the high excitation intensity enhancement created by plasmonic coupling[27], but can also be viewed as an improvement of the third-order ITO susceptibility $\chi^{3\omega}$ (see Supplementary Section 6 for details). Exploiting the experimental data, we compute a third-order effective susceptibility of 3,543 nm^2 V^{-2} for the 25 nm ITO nanoparticle decorated with the plasmonic dimer, which is a susceptibility seven orders of magnitude higher than those reported with nonlinear macroscopic crystals[28].

As non-negligible intrinsic third-harmonic responses from plasmonic antennas were recently reported[17–19], careful attention has been devoted to quantify the intrinsic third-harmonic background from the plasmonic dimers by conducting extensive sets of multiwavelength measurements (for data see Supplementary Section 4) and nonlinear FDTD simulations for the limiting cases with either $\chi^{(3)}_{Au}$ or $\chi^{(3)}_{ITO}$ set to zero (for data see Supplementary Section 8). These results, combined with a gap size dependence analysis and an extensive set of multiwavelength measurements, indicate that THG from the ITO nanoparticle coupled to the plasmonic dimer is 16 times higher (THG upconversion efficiency three orders of magnitude higher; for data see Supplementary Section 4) than the THG background from the metallic dimer itself, thus confirming that the nonlinear signal mainly originates from ITO[29].

The nonlinear phenomenon responsible for the upconversion process requires the instantaneous capture of three infrared photons to generate a green photon, hence a cubic dependence of the radiated third harmonic with excitation intensity is expected. This trend is corroborated by the experimental measurements presented in Fig. 2c, which show that the THG intensity from the upconversion hybrid system is sensitive to the third power of the fundamental incident light. Unlike luminescent nanocrystals[3], the upconverted light from the hybrid nanosystem does not exhibit any saturation limitation; on the contrary, increasing the fundamental incident power leads to an improvement in the conversion efficiency. This observation is a direct consequence of the scattering nature of harmonic generation mechanisms as opposed to the absorption nature of luminescence processes. The current limitation regarding the nonlinear upconversion efficiency is related to the laser damage threshold of the hybrid nanosystems, which prevents achieving third-harmonic conversion efficiency greater than 7×10^{-4}% (for more discussions see Supplementary Section 7).

As an immediate application of high relevance for nanophotonics, we accurately quantified the excitation intensity enhancement η for various nanodimers (Fig. 3a) with their gaps coupled to single emitters, by using an ITO nanoparticle as a probe of the near-field plasmonic intensity. From the numerical simulations presented in Fig. 3b, one can observe that any increase in the dimer gaps leads to a reduction in the plasmonic intensity enhancement, and therefore to weaker third-harmonic responses from the ITO nanoparticle. Such expectations are corroborated by the third-harmonic spectral measurements shown in Fig. 3c,e, where the THG intensity drastically decreases with increasing gap dimensions. Exploiting these data, the intensity enhancement factor η can be computed as the cube root of the ratio between the third-harmonic power from the ITO nanoparticle with and without the plasmonic antenna under investigation. This is discussed further in Supplementary Section 5. The experimental values determined for η are presented in Fig. 3d,f together with numerical predictions. Excellent agreement was found between the experimental observations and the simulated data for all probed designs. As expected from the third-harmonic spectra of Fig. 2b and Fig. 3c,e, the highest intensity enhancements are provided by the 35-nm-gap nanorod and 30-nm-gap nanocylinder dimers, with experimental values for η of 103.6 and 49.4, respectively, and numerical predictions of 119.5 and 55.1, respectively. Lower enhancement factors were measured for the 55-nm-gap nanorod and 40-nm-gap nanocylinder dimers due to weaker electromagnetic couplings for increasing gaps. These excellent agreements between experimental and numerical intensity enhancements demonstrate that single nonlinear nanoparticles can play the role of subwavelength near-field probes.

In summary, we have introduced and experimentally highlighted the viability of a nanoscale upconversion system based on a single nonlinear nanometric particle decorated with a plasmonic motif. This nanosystem provides nonlinear upconversion enhancements of up to 10^6-fold compared with an isolated ITO nanoparticle, and enables the unambiguous discrimination of the nonlinear signal emitted by the ITO nanoparticle from the intrinsic nonlinear metallic background. Although the plasmonic antennas presented here exhibit narrowband resonances, tunable third-harmonic upconversion nanosystems could be realized by implementing a nonlinear nanomaterial at the gap of broadband plasmonic antenna designs[30]. Finally, we demonstrated that a nonlinear nanoparticle can be used as a near-field nanoprobe to quantify the hotspot intensities in plasmonic dimers when single emitters are placed at their gaps, thus introducing a new form of nonlinear enhanced light–matter interaction at the nanoscale and bridging the gap between the theoretical predictions of field enhancement and experimental electromagnetic nanometrology.

Methods

Sample fabrication. The third-harmonic upconversion nanosystems composed of an ITO nanoparticle decorated with a plasmonic dimer were realized by means of electron-beam lithography with etch-down and lift-off approaches, accompanied by precise alignments. Indeed, a pure lift-off approach prevents the achievement of nanometric-size particles with diameters smaller than 30 nm via sputtering, because of its non-directional deposition nature. Accordingly, a quartz substrate was first covered with a 40 nm ITO film by sputtering. High-resolution circular nanodots and alignment markers were then defined in hydrogen silsesquioxane resist on the substrate by electron-beam lithography. Ion-beam etching (argon ions) of the ITO layer was then performed to generate single 25-nm-diameter nanoparticles, as presented in Fig. 1b. The sample was next coated with polymethylmethacrylate, and rod/cylinder nanodimer shapes centred on a single ITO nanoparticle were defined in the resist, followed by thermal evaporation of a 2 nm chromium adhesion layer and 40 nm gold. A final lift-off step led to the completion of the upconversion system, comprising an ITO nanoparticle trapped in the gap of a plasmonic dimer (Fig. 1b,c). More details about sample fabrication are provided in Supplementary Section 1.

Numerical simulations. We performed three-dimensional FDTD simulations using the commercial software FDTD solution v8.6 (Lumerical). SEM images of the dimers were imported into the software to generate the dimer model according to the fabricated dimensions. The ITO nanoparticles were considered to be ideal 25-nm-diameter cylinders, located according to the SEM pictures. The optical dielectric functions of the different materials—Au, Cr, SiO_2 and ITO—were taken from tabulated data[24,25]. The dielectric dispersion of the materials was fitted in the spectral range 1,000–2,000 nm by a six-coefficient model, allowing a tolerance of 0.1 and enforcing passivity.

All simulation boundaries were set as perfect matched layers to replicate a single dimer over a semi-infinite substrate scenario. The solver-defined TFSF source was used to reduce computation effort, as it allows definition of the plane-wave excitation within the volume enclosing only the dimer. For the linear simulations shown, the TFSF box had dimensions of 800 nm × 500 nm × 80 nm. The x-polarized plane-wave excitation was incident normal to the dimer from the semi-infinite free space, that is, propagating along $-z$. The incident temporal pulse had spectral components ranging from 1,000 nm to 2,000 nm (that is, central wavelength of 1,500 nm and bandwidth of 1,000 nm) and a pulse length of ~6.64 fs. A conformal non-uniform mesh was used to accurately map the details of the model. The TFSF volume default grid was 7 nm × 7 nm × 2 nm. For the dimer region, the volume with dimensions of 650 nm × 340 nm × 50 nm was discretized with a cubic grid of 4 nm × 4 nm × 2 nm. An even smaller cubic grid of 0.5 nm × 0.5 nm × 2 nm was overridden in the region enclosing the ITO nanoparticle and the gaps between the ITO particle and each arm of the dimer. A finer mesh size along z of 0.5 nm was applied for the chromium layer. The maximum simulation time was set to 300 fs. The time-stepping stability factor was set to 0.99, which corresponds to a time step of $\delta t = 0.00095$ fs. The residual energy in the simulation box volume was at least 50 dB lower than its peak value to ensure that the continuous-wave information obtained by discrete Fourier transformations was valid. A standard convergence test was performed to ensure negligible numerical errors originating from the perfect-matched-layer distance, non-uniform meshing or monitor sampling.

The extinction cross-section was calculated from the sum of the power flowing outward through a volume enclosing the TFSF source (scattering cross-section) and the net power flowing inward through a rectangular cuboid inside the TFSF volume enclosing the dimer (absorption cross-section). The average intensity within the ITO nanoparticle was obtained from a three-dimensional field monitor. To generate the intensity enhancement colour maps, a two-dimensional field profile monitor recorded the field on the x–y middle cross-section plane. More linear and nonlinear simulations are presented in Supplementary Section 8.

Experimental set-up. The inverted microscope developed for this work made use of a Yb:KGW femtosecond PHAROS laser system as the pump of a collinear optical parametric amplifier ORPHEUS with a LYRA wavelength extension option (Light Conversion; pulse duration 140 fs, repetition rate 100 kHz). For nonlinear experiments, the fundamental incident wavelength was focused on the sample plane by a 0.6 NA microscope objective, and the backward-emitted third-harmonic generation at 500 nm was collected with the same objective. More information about the experimental set-up is provided in Supplementary Section 3.

Received 12 October 2013; accepted 22 January 2014; published online 9 March 2014

References

1. Débarre, D. *et al.* Imaging lipid bodies in cells and tissues using third-harmonic generation microscopy. *Nature Methods* **3,** 47–53 (2006).
2. Zhou, J., Liu, Z. & Li, F. Upconversion nanophosphors for small-animal imaging. *Chem. Soc. Rev.* **41,** 1323–1349 (2012).
3. Zou, W. Q., Visser, C., Maduro, J. A., Pshenichnikov, M. S. & Hummelen, J. C. Broadband dye-sensitized upconversion of near-infrared light. *Nature Photon.* **6,** 560–564 (2012).

4. Agio, M. & Alù, A. *Optical Antennas* (Cambridge Univ. Press, 2013).
5. Kauranen, M. & Zayats, A. V. Nonlinear plasmonics. *Nature Photon.* **6,** 737–748 (2012).
6. Novotny, L. & van Hulst, N. Antennas for light. *Nature Photon.* **5,** 83–90 (2011).
7. Franken, P. A., Hill, A. E., Peter, C. W. & Weinreich, G. Generation of optical harmonics. *Phys. Rev. Lett.* **7,** 118–119 (1961).
8. Xie, X. S., Yu, J. & Yang, W. Y. Living cells as test tubes. *Science* **312,** 228–230 (2006).
9. Tian, G. *et al.* Mn^{2+} dopant-controlled synthesis of $NaYF_4$:Yb/Er upconversion nanoparticles for *in vivo* imaging and drug delivery. *Adv. Mater.* **24,** 1226–1231 (2012).
10. Wang, H-Q., Batentschuk, M., Osvet, A., Pinna, L. & Brabec, C. J. Rare-earth ion doped up-conversion materials for photovoltaic applications. *Adv. Mater.* **23,** 2675–2680 (2011).
11. Lamprecht, B., Krenn, J. R., Leitner, A. & Aussenegg, F. R. Resonant and off-resonant light-driven plasmons in metal nanoparticles studied by femtosecond-resolution third-harmonic generation. *Phys. Rev. Lett.* **83,** 4421 (1999).
12. Mühlschlegel, P., Eisler, H-J., Martin, O. J. F., Hecht, B. & Pohl, D. W. Resonant optical antennas. *Science* **308,** 1607–1609 (2005).
13. Schuck, P. J., Fromm, D. P., Sundaramurthy, A., Kino, G. S. & Moerner, W. E. Improving the mismatch between light and nanoscale objects with gold bowtie nanoantennas. *Phys. Rev. Lett.* **94,** 017402 (2005).
14. Cai, W., Vasudev, A. P. & Brongersma, M. L. Electrically controlled nonlinear generation of light with plasmonics. *Science* **333,** 1720–1723 (2011).
15. Abb, M., Albella, P., Aizpurua, J. & Muskens, O. L. All-optical control of a single plasmonic nanoantenna–ITO hybrid. *Nano Lett.* **11,** 2457–2463 (2011).
16. Kim, S. *et al.* High-harmonic generation by resonant plasmon field enhancement. *Nature* **453,** 757–760 (2008).
17. Hanke, T. *et al.* Tailoring spatiotemporal light confinement in single plasmonic nanoantennas. *Nano Lett.* **12,** 992–996 (2012).
18. Hentschel, M., Utikal, T., Giessen, H. & Lippitz, M. Quantitative modeling of the third harmonic emission spectrum of plasmonic nanoantennas. *Nano Lett.* **12,** 3778–3782 (2012).
19. Melentiev, P. N., Afanasiev, A. E., Kuzin, A. A., Baturin, S. A. & Balykin, V. I. Giant optical nonlinearity of a single plasmonic nanostructure. *Opt. Express.* **21,** 13896–13905 (2013).
20. Koller, D. M. *et al.* Superresolution Moiré mapping of particle plasmon modes. *Phys. Rev. Lett.* **104,** 143901 (2010).
21. Dregely, D., Neubrech, F., Duan, H., Vogelgesang, R. & Giessen, H. Vibrational near-field mapping of planar and buried three-dimensional plasmonic nanostructures. *Nature Commun.* **4,** 2237 (2013).
22. Bermúdez Ureña, E. *et al.* Excitation enhancement of a quantum dot coupled to a plasmonic antenna. *Adv. Mater.* **24,** OP314–OP320 (2012).
23. Liu, N. *et al.* Individual nanoantennas loaded with three-dimensional optical nanocircuit. *Nano Lett.* **13,** 142–147 (2013).
24. Palik, E. D. *Handbook of Optical Constants of Solids* (Academic, 1985).
25. Humphrey, J. L. & Kuciauskas, D. Optical susceptibilities of supported indium tin oxide thin films. *J. Appl. Phys.* **100,** 113123 (2006).
26. Alaverdyan, Y. *et al.* Spectral tunability of a plasmonic antenna with a dielectric nanocrystal. *Opt. Express* **19,** 18175–18181 (2011).
27. Giannini, V., Fernández-Domínguez, A. I., Heck, S. C. & Maier, S. A. Plasmonic nanoantennas: fundamentals and their use in controlling the radiative properties of nanoemitters. *Chem. Rev.* **6,** 3888–3912 (2011).
28. Ganeev, R. A., Kulagin, I. A., Ryasnyansky, A. I., Tugushev, R. I. & Usmanov, T. Characterization of nonlinear optical parameters of KDP, $LiNbO_3$ and BBO crystals. *Opt. Commun.* **229,** 403–412 (2004).
29. Harutyunyan, H., Volpe, G., Quidant, R. & Novotny, L. Enhancing the nonlinear optical response using multifrequency gold-nanowire antennas. *Phys. Rev. Lett.* **108,** 217403 (2012).
30. Navarro-Cia, M. & Maier, S. A. Broad-band near-infrared plasmonic nanoantennas for higher harmonic generation. *ACS Nano* **6,** 3537–3544 (2012).

Acknowledgements

The authors thank A. Rakovich for fabrication of preliminary samples, Y. Sonnefraud for help with sample characterization and V. Giannini and A. I. Fernández-Domínguez for discussions. This work was funded by the Engineering and Physical Sciences Research Council (EPSRC) through the Active Plasmonics programme, the Leverhulme Trust, the US Army International Technology Centre Atlantic (USAITC-A) and the Office of Naval Research (ONR and ONR Global). M.N-C. is supported by an Imperial College Junior Research Fellowship.

Author contributions

H.A. and S.A.M. conceived and supervised the project. M.N-C. provided the numerical work, M.R. fabricated the samples and H.A. performed the experiments. H.A. wrote the manuscript. All authors participated in data processing, analysis, discussions and manuscript preparation.

Additional information

Supplementary information is available in the online version of the paper. Reprints and permissions information is available online at www.nature.com/reprints. Correspondence and requests for materials should be addressed to H.A.

Competing financial interests

The authors declare no competing financial interests.